Nanoscale Advances

ROYAL SOCIETY OF CHEMISTRY

PAPER

View Article Online
View Journal | View Issue

Cite this: *Nanoscale Adv.*, 2023, **5**, 485

Ultrafast hot-carrier cooling in quasi freestanding bilayer graphene with hydrogen intercalated atoms†

Sachin Sharma,[a] Rachael L. Myers-Ward,[b] Kurt D. Gaskill[c] and Ioannis Chatzakis *[a]

Femtosecond-THz optical pump probe spectroscopy is employed to investigate the cooling dynamics of hot carriers in quasi-free standing bilayer epitaxial graphene with hydrogen interacalation. We observe longer decay time constants, in the range of 2.6 to 6.4 ps, compared to previous studies on monolayer graphene, which increase nonlinearly with excitation intensity. The increased relaxation times are due to the decoupling of the graphene layer from the SiC substrate after hydrogen intercalation which increases the distance between graphene and substrate. Furthermore, our measurements show that the supercollision mechanism is not related to the cooling process of the hot carriers, which is ultimately achieved by electron optical phonon scattering.

Received 2nd October 2022
Accepted 16th December 2022

DOI: 10.1039/d2na00678b

rsc.li/nanoscale-advances

Introduction

For over a decade, graphene has been among the most widely explored optoelectronic materials.[1,2] A large number of investigations have established the significance of graphene in photodetection, data communication, biosensors, ultrafast systems and THz technology and more, due to high mobility of the carriers and the strong interaction of light over an extraordinary broad spectral range.[1–15] These applications rely on the optoelectronic properties of graphene that are determined by the dynamics of the energy relaxation of the hot carriers. Thus, understanding the mechanisms that contribute to the relaxation processes is pivotal. Because pump-probe spectroscopy is an excellent tool to probe relaxation processes, many experiments exploiting this technique using different combinations of pump and probe wavelengths ranging from visible to terahertz (THz) region have been reported. Such experiments commonly use THz pump-probe spectroscopy where carrier excitation is triggered with an optical or near infrared radiation (NIR) pulse and subsequently the carrier dynamics are observed by recording the THz transmission through the material for different time delays.[16–22] Since the THz photon energy is a few meV, this is significantly smaller than the Fermi energy for most graphene samples. Consequently, THz (probe-field) contribution to the carrier excitation can be ignored and the inter-band processes can be exclusively associated with the excitation (pump) pulse. The ultrafast optical-pump THz-probe spectroscopy is a very successful method to study the nonequilibrium dynamics of hot carriers and phonons and has been extensively applied to a wide variety of materials including other carbonic materials such as carbon nanotubes for investigating intra-excitonic transitions[23] and phonon dynamics.[24] At room temperature, carrier relaxation in graphene is extremely fast and typically occurs on a time scale of a few picoseconds.[8,16–20,25–38] When the pump pulse arrives on a graphene sample it creates a highly nonequilibrium "hot" electron distribution, which first relaxes on an ultrafast time scale on order of tens of femtoseconds to a thermalized Fermi-Dirac distribution with a characteristic temperature T_e. The relaxation of the hot carriers is primarily controlled by electron–electron (e–e) interactions that are sensitive to the doping. Subsequently electrons slowly cool down, either *via* coupling to optical phonons (at Γ and K-point of the Brillouin zone) that are coupled to acoustic phonon,[39] or by direct coupling of hot electrons to acoustic phonon[40] giving large decay times (few hundred ps that are not relevant to our observations). Additional studies at low electron temperatures emphasized the role of the disorder as a source of momentum needed for direct coupling of hot carriers to acoustic phonons *via* supercollision (SC) scattering.[27,41–44] Another scenario for cooling includes the interaction of hot carriers with phonons of a polar substrate.[45] In the optical pump THz-probe experiment the relative long THz-pulse width (~1 ps) compared to the carrier–carrier scattering time of a few hundred fs cannot be resolved. Instead, the long decay of the quasi-equilibrium Fermi–Dirac distribution can be effectively probed. Various experimental studies have been also conducted using this method to investigate the sign of the transient conductivity from hot carriers and the role the

[a]Texas Tech University Department of Physics & Astronomy, Lubbock, Texas TX, 79409, USA. E-mail: Ioannis.chatzakis@ttu.edu

[b]U.S. Naval Research Laboratory, Washington, DC20375, USA

[c]Institute for Research in Electronics and Applied Physics, University of Maryland, College Park, MD, USA

† Electronic supplementary information (ESI) available: Details on the supercollision model. See DOI: https://doi.org/10.1039/d2na00678b

Fermi energy plays in the relevant process. These experiments utilize THz photoconductivity deduced from THz transmission among pumped and unpumped high-mobility graphene samples[16,20] and have shown that THz photoconductivity can both be negative and positive. Shi *et al.*,[16] demonstrated that hot carriers in graphene lead to an unusual conductivity behaviour that can be switched from semiconductor-like to metal-like response depending on the doping level of the sample. It has been also showed by Tierlooij *et al.*,[46] that induced THz transient transparency can be obtained by heating the carriers in graphene using optical excitation, and Jnawali *et al.*,[18] showed that within the Drude model, this increase in the THz transmission is due to the increased scattering rate of hot electrons. It was claimed that these observations were due to optical phonon scattering and carrier heating effects, however, a full justification is lacking. These claims were addressed in a comprehensive study by Tomadin *et al.*,[17] where carrier dynamics and photoconductivity of graphene were reported for varying Fermi energies. Tomadin concluded that the sign of photoconductivity is determined by the type of electronic transitions. In case of low E_F, interband transitions dominate over intraband transitions and *vice versa* is true for high E_F. Winnerl *et al.*,[30,47] performed diverse experiments using multilayer epitaxial graphene (70 layers) with different combinations of pump and probe pulses ranging from 10 to 250 meV. They observed a slower relaxation dynamic for excitation energies <160 meV (*K*-point phonons) above the Fermi energy, but with the optical phonon still playing important role. Mihnev *et al.*,[25] demonstrated that interlayer Coulomb coupling in multilayer epitaxial graphene (more than 60 layers samples were used) provides a cooling mechanism for the hot carriers.[25] Also, electrical transport measurements have been used and optical phonon-mediated carrier cooling mechanisms have been identified. However, this mechanism is relevant only for carriers at high temperature. For electron temperatures $T_e \ll T_F$ supercollisions plays significant role in the relaxation process.

Nonetheless, while the energy relaxation in graphene prepared either by CVD or exfoliation method has been extensively studied, much less literature exist for epitaxial graphene (EG) on SiC substrate. Particularly of interest is hydrogen intercalated EG. For standard epitaxial graphene on the SiC surface, the first graphene layer, called buffer layer or zero-layer graphene (ZLG), is between the SiC substrate and the epitaxial graphene. The ZLG is bound to the SiC substrate (Fig. 1 Top Left) and strongly interacts with the substrate *via* the p_z orbitals thus, the π bands with the characteristic linear dispersion of graphene cannot be developed. A true monolayer of graphene, which possess typical graphene band structure, can be formed

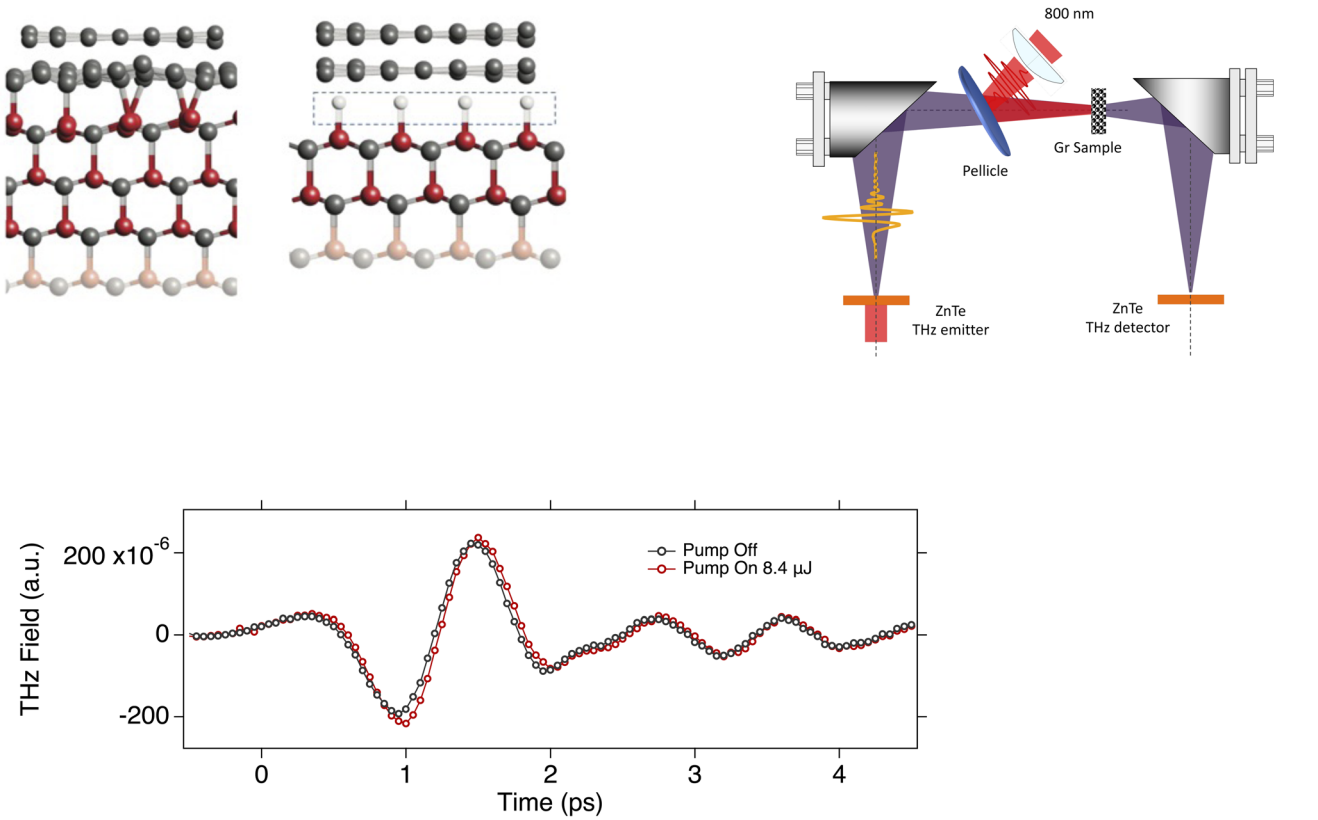

Fig. 1 (Top Left) The graphene layer on SiC surface. The Left panel shows the graphene layer with the ZLG (buffer) before the H-intercalation. Si are bonded with the C- of graphene. The Right panel depicts the final stage of the graphene configuration with the intercalated hydrogen shown as the small white balls that saturate the Si bonds. (Top Right) schematic representation of the experimental setup we used in this study. (Bottom) the THz pulse transmitted through the 6H–SiC with the graphene on top with pump on and pump off. The small phase shift is related to some scattering time.

on top of the buffer by further annealing of the sample. It has been demonstrated[48–50] by different groups that the buffer layer and the monolayer can be decoupled from the substrate by hydrogen atoms intercalation as it is shown in Fig. 1. With the intercalation method, large areas of high-quality quasi free-standing graphene can be produced for practical applications, thus it is critical to understand its carrier cooling mechanisms.

In this work we explore the cooling dynamics of hot carriers in H-intercalated quasi free standing bilayer graphene utilizing ultrafast pump-probe THz spectroscopy. We demonstrate (i) a significant deviation from the supercollision cooling mechanism and, (ii) that the relaxation of the hot carriers mostly occurs due to electron–optical phonon interactions. In accordance with previous measurements, we also observe an increase of the pump induced conductivity, $\Delta\sigma$, and of the relaxation time with the excitation fluence.

In quasi free standing epitaxial graphene, the graphene layer is sitting on top of a graphene-like carbon layer which forms a large unit-cell superstructure with a $(6\sqrt{3} \times 6\sqrt{3})R30^0$ periodicity, called buffer layer or zero-layer graphene (ZLG). The ZLG has same geometrical atomic arrangement as graphene. However, about 30% of the carbon atoms in ZLG, are covalently bound to the top of Si atoms of the SiC surface which prevents the formation of the linear dispersion of π bands typical for graphene, so that the latter cannot be observed by ARPES[50] (see Fig. 1(a)). Thus, the ZLG lacks bands with linear dispersion and is electronically inactive. With the penetration of the hydrogen atoms under the ZLG, the bonds between the C and the Si break and the Si dangling bonds are saturated with hydrogen atoms as shown in Fig. 1(a). The Si–H bonds are electronically inactive and the inetrface between SiC–graphene is expected to be defects free. The ZLG turns to quasi free-standing epitaxial graphene (QFSEG) and the monolayer graphene turns to into a decoupled bilayer.[51] Presumably the reduced mobility in epitaxial graphene is due to presence of the dangling bonds between the C and Si atoms. By breaking these covalent bonds, a QFSEG that possess the typical graphene structure, can be obtained. Riedl *et. al.*,[50] demonstrated that the elimination of the covalent bonds to decouple the epitaxial graphene layers from the substrate can be achieved by intercalation of hydrogen atoms between the ZGL and the SiC. Because the epitaxial graphene doesn't grow as a simple AB staked graphite films but with high density of rotational faults, the adjacent layers are rotated relative to each other. Hass *et. al.*,[52] demonstrated by first principles calculations that the adjacent rotated layers become electronically decoupled, preserving the linear band structure at the *K*-point and thus the bilayer graphene behaves as an isolated graphene sheet. Epitaxial graphene on SiC reveals a pronounce n-type doping that can be explained by electron transfer from, interface (SiC/graphene) density of states associated with carbon or silicon dangling bonds to the graphene layer.

After the intercalation of hydrogen graphene exhibits a strong p-type doping, with a Fermi energy usually few hundreds meV. The change of the doping type from n to p is due to spontaneous polarization[53] that it is an intrinsic characteristic of the most SiC polytypes. It should be noted that the type of doping n or p depends on the polytypes of the SiC, *e.g.* the p-type character vanishes for the quasi free standing graphene when going from the hexagonal SiC to the cubic 3C polytype which is due to spontaneous polarization of the SiC substrate.[53]

Experimental details

The laser source was a 1 kHz Ti:Sapphire regenerative amplifier system that produced 7 mJ, 100 fs pulses centered at 800 nm. A part of the output of the laser amplifier was used to generate and detect the THz radiation. Quasi-single cycle THz pulses with bandwidth ~2.3 THz centered at 1.2 THz generated *via* optical rectification in a 1 mm thick ZeTe (110) nonlinear crystal. The emitted THz radiation was focused on the graphene samples by an off-axis parabolic mirror at normal incidence. The spot size of the THz beam on the sample was about 0.7 mm, measured by the knife-edge method. The transmitted radiation through the sample was collected and refocused by parabolic mirrors onto a second 1 mm thick ZnTe (110) crystal and detected by electro-optic sampling (EOS) method.[46] Another part of the laser beam was used as a sampling beam that was scanned *via* an adjustable optical delay line and was used to sample the temporal electric field profile of the THz transients. Schematic illustartion of the optical-pump THz-probe measurement technique is shown in Fig. 1. All the measurements were performed at room temperature. A phased-locked chopper in combination with a lockin-amplifier was used in the pump path to modulate the beam at 500 Hz to reduce the noise of the signal. The photon energies of the pump pulses we used to excite the graphene samples was 1.55 eV (800 nm) and the excitation fluence in the range of 27 to 270 μJ cm^{-2}. The spot size of the pump beam was 2 mm to ensure uniform excitation of the probed area. The pump-induced changes in the THz transmission were measured by scanning a second optical delay line that introduces a time-delay between the near infrared (NIR) pump pulse and the maximum amplitude of the THz probe pulses.

The samples we used in this study was pH-doped quasi freestanding epitaxially grown bilayer graphene on hexagonal SiC semi-insulating substrate with hydrogen intercalated atoms. To determine the sheet carrier density and mobility, we performed Hall measurements (see ESI†) and found $(9.14 \pm 0.11) \times 10^{12}$ cm^{-2} and determined $\mu = (4291 \pm 66)$ cm^2 V^{-1} s^{-1} respectively that are typical values for quasi free standing bilayer graphene on 6H–SiC substrate.[54,55] The carrier density we found corresponds to Fermi energies $E_F = 0.38$ eV.

Results and discussion

To characterize the THz conductivity of the unexcited sample we recorded the time dependent THz electric fields transmitted through the quasi-freestanding graphene on the SiC substrate denoted as $E_{gr}(t)$, and through of a blank SiC substrate similar to the one used for the graphene, denoted $E_{ref.}(t)$ in order to normalize the data. Typical time-domain THz electric-fields

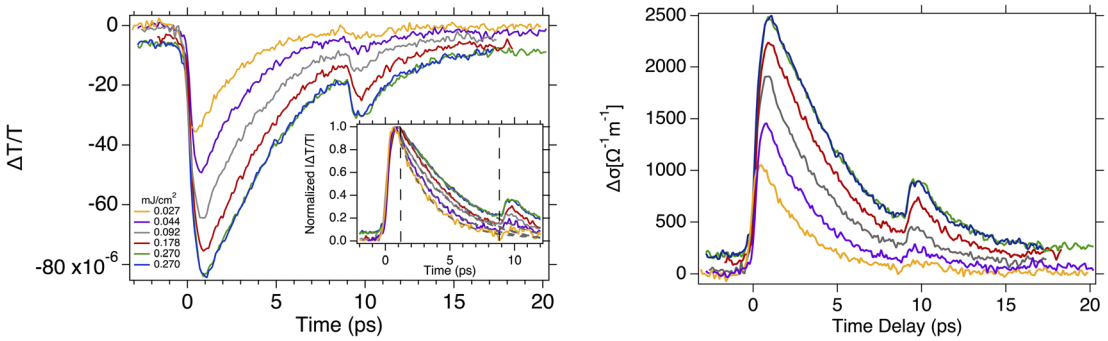

Fig. 2 Ultrafast time resolved optical-pump THz probe spectroscopy on quasi freestanding bilayer graphene. (Left panel) differential THz transmission spectra $\Delta T/T$ recorded at different pump fluences ranging from 27 to 270 μJ cm^{-2} and 295 K substrate temperature. The inset shows the normalized absolute value of the differential transmission. The gray dashed lines are the fits to mono-exponential function. The vertical dashed lines define the time window where the fit was restricted. (Right panel) the corresponding changes in conductivity are shown.

transients $E_{gr}(t)$ and $E_{ref.}(t)$ are shown in Fig. 1. The THz field complex transmission coefficient $T^*(\omega)$ is obtained from the ratio between the two Fourier transformed spectra $E_{gr}(t)$ and $E_{ref.}(t)$. We derive the complex transmission coefficient as $T^*(\omega) = |T(\omega)|e^{i\varphi(\omega)}$, where $|T(\omega)|$ and $\varphi(\omega)$ are the amplitude and the phase, respectively. Applying the thin-film approximation,[1–3] we have,

$$T^*(\omega) = \frac{E^*_{gr}(\omega)}{E^*_{ref.}(\omega)} = \frac{1+n}{1+n+NZ_0\sigma(\omega)} \quad (1)$$

In eqn (1), $n = 3.124$ is the refractive index of the SiC substrate. The number of the graphene layers is denoted by N, and $Z = 377\ \Omega$ is the vacuum impedance. To get insight into the graphene response under photoexcitation conditions a pump pulse was focused on the graphene at a spot size of 2 mm determined by a metallic aperture placed in front of the sample. The pump photon energies E_{ph} was 1.55 eV to excite electrons/holes in conduction/valence band states with energies $|E_{ph}|$ above/below the Dirac point. We probe the pump-induced change in the transmission of the THz pulse after a time delay of ~400 fs that is much longer than the thermalization time of the electronic distribution, so the electronic system is in a quasi-equilibrium state. To obtain the photoinduced conductivity of the graphene samples, we directly recorded the pump-induced changes of the THz-waveform peak amplitude transmission $(\Delta T(t)/T_0) = (T_{\text{Pump ON}} - T_{\text{Pump OFF}})/T_{\text{Pump OFF}}$, by placing the chopper in the pump path and normalized to the THz transmission without photo-excitation. For thin samples the differential transmission $(\Delta T/T_0)$ is related to the photoinduced conductivity by the relation.[18]

$$\Delta\sigma = \frac{1+n}{Z_0}\left(-\frac{\Delta T}{T_0}\right)\left(\frac{1}{1+\Delta T/T_0} - 1\right) \quad (2)$$

The negative change of the transmission $(-\Delta T/T_0)$ we measured here indicates $\Delta\sigma > 0$, *i.e.* the conductivity increases as a result of the photoexcitation, similar to what has been observed in previous studies on monolayer graphene.[16] However, in contrast to previous studies on monolayer graphene, our measurements do not show that the supercollision mechanism is relevant to the cooling process of the hot carriers, as it will be discussed later in details. To investigate the relaxation dynamics in graphene we record the $\Delta T(t)$ as a function of probe delay time τ. Fig. 2 illustrates the corresponding data. For all excitation fluences we used in this study the THz transmission increases rapidly in about 1 ps after photoexcitation and then recovers the initial value within few picoseconds. The max amplitude of the corresponding photo-induced conductivity extracted form Fig. 2 (Right panel) is also shown in Fig. 3(d). The decrease of the transparency of the graphene after the photoexcitation corresponds to an increase of the conductivity due to the increase of the conducting carrier concentration. This effect occurs in conventional semiconductors with photoexcitation. However, the opposite effect has also been observed where the increase of the ΔT results in decreased conductivity, which is due to increased carrier scattering rate.[18] In the context of the electronic temperature, in conventional semiconductors the increase of the T_e implies increase of the conductivity through the increase of the Drude weight D. In graphene the Drude weight D is given by

$$D = G_0 2k_B T_e\left[2\cosh\left(\frac{E_F}{2k_B T_e}\right)\right] \quad (3)$$

where E_F is the Fermi energy, k_B is the Boltzmann constant, and T_e is the electron temperature.

The contributions from the Drude weight and the scattering rate depends on the initial Fermi energy and a positive or negative conductivity. In Fig. 2 (Left) are depicted typical results of the time-domain transient transmission of THz pulses through graphene at different excitation fluences ranging from 27 to 270 μJ. The dynamical traces we recorded show sub picosecond rise time followed by few picoseconds decay time. The experimental data were fitted using a mono-exponential function $-\Delta T/T_0 = C\exp(-t/\tau_d)$ where, τ_d is the cooling time constant that we found it as of 2.6 to 6.4 ps for the lowest and highest excitation fluences we used, respectively. The longer decay constant observed here is due to hydrogen intercalation that causes the decoupling of graphene and, its vertical displacement by ~0.21 nm[48] from the SiC substrate. Mihnev's

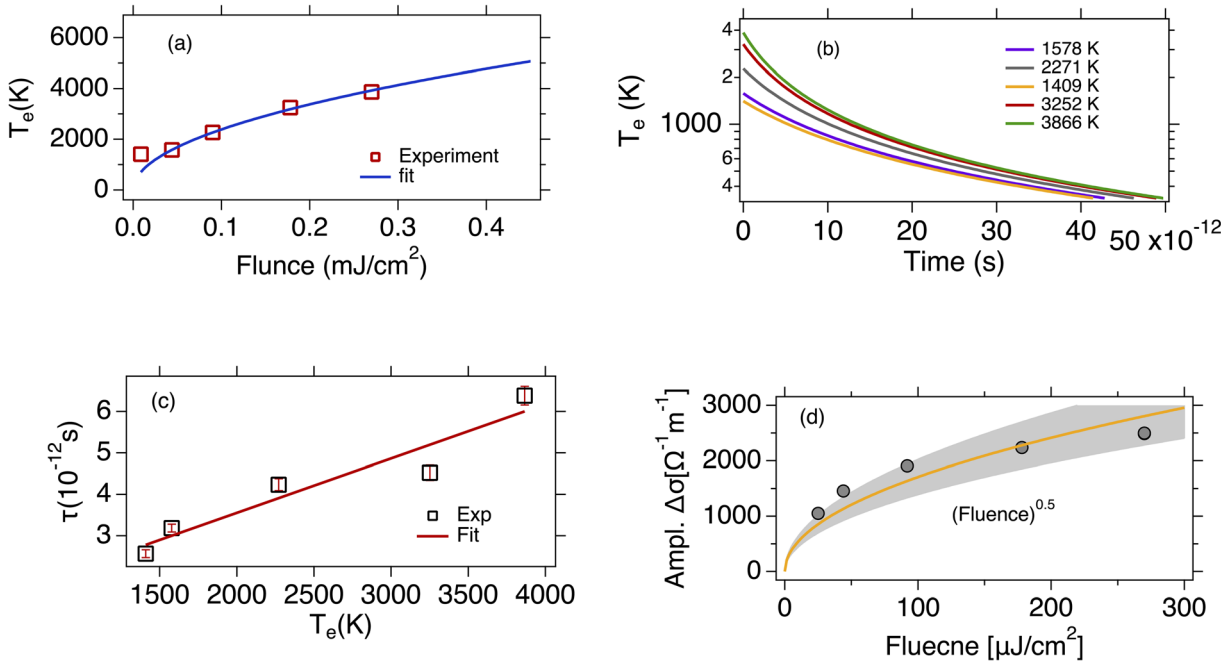

Fig. 3 (a) The initial electron temperature is plotted as a function of the excitation fluence. The blue line is the fit with the square root function. (b) The dynamics of the electron temperature calculated from eqn (5) (see text) as a function of the time delay in a semi log plot. Different color represents different initial temperature of the electrons. The significant deviation of the disorder-assited cooling of carriers model (super-collisions mechanism) from the monoexponental function, confirms that the supercollisions is not the dominant mechanism in the cooling process. (c) The carriers cooling time plotted as a function of the electron initial temperature. The red solid line is a linear fit to the experimental data, (d) the max amplidute of the pump induced conductivity is plotted as afunction of the excitation fluence. The data are fitted with the square root function shown by the yellow solid line and the gray shaded area is the confidence interval.

et. al.,[25] demonstrated that the heat transfer from one layer graphene to another is due to the coulomb interaction between electrons in different layers, and that a decoupling of the layers will lead to the reduced heat transfer rate. Thus, the reduced coupling due to broken covalent bonds between the graphene and the substrate we observed in our samples, naturally causes a decrease in the cooling rate. The secondary peak at about 10 ps is due to round trip of the excitation pulse inside the SiC substrate that re-excites the graphene. As seen at ~10 ps where the secondary peak rises, the cooling of the carriers has not be completed. Thus, to deduce the decay time constants we limit the exponential fit to the time window between ~1 ps to ~9 ps excluding the secondary peak, in order to avoid any influence on the dynamics from the back-reflected excitation pulse. As shown in Fig. 2 (Left) in the first ~1 ps the negative terahertz transmission $\Delta T/T$ decreases after photoexcitation, but the corresponding conductivity increases (increase of D) and has a positive sign. This is mainly due to two reasons. First, the increases the conductivity is due to the higher density of free carriers in the conduction band created by photoexcitation. Second, due to the temperature dependence of the conductivity, the absorption of the pump energy causes an increase in the temperature of the electrons leading to a higher conductivity (see eqn.(3)).

Beyond few picoseconds a decrease in the photogenerated carrier density occurs as the carriers cool down, that results in an increase of the transmission but the opposite occurs in the conductivity as it is shown in Fig. 2 (Right). For excitation energies above the Fermi energy once the quasi-Fermi Dirac distribution is realized after the photoexcitation, it is typical to justify the cooling process predominantly *via* optical phonons (will be discussed later) rather than acoustic phonons. This is a faster process and at 295 K, is widely reported to take few picoseconds.[18] In addition, the relatively weaker acoustic phonon coupling also contributes and leads to significantly longer decay times (hundreds of ps),[40] that are not relevant to time scales we deduced in this study. We infer from the experimental data in Fig. 2 longer decay times by more than of a factor of two, comparable to the decay times observed in monolayer graphene in previous studies.[34] In our quasi-free-standing graphene samples, due to presence of the intercalated hydrogen atoms, there are not additional bonds between ZLG and SiC substrate, a decoupling between graphene and substrate occurs converting the ZLG into a new graphene layer as shown in Fig. 1. The same reason applies for the weak or even non-existent contribution of the substrate phonons to the cooling process of the energy of the hot carriers.

To get further insight into hot carriers cooling we examine the fluence dependence of the photoinduced THz conductivity $\Delta\sigma$. Based on our experimental conditions, $\Delta\sigma$ is proportional to the electron temperature. Using the electronic heat capacity C_e and assuming a small fraction η of the incident power density is absorbed by the sample, we can calculate the initial hot electron temperature T_e. For highly doped graphene we have $\alpha = \frac{C_e}{T}$

with $\alpha = (2\pi/3)k_B^2 \frac{E_F}{(\hbar v_F)^2}$, which is the heat capacity coefficient. Then for the hot electron temperature

$$T_{e,0} = T_L\sqrt{1 + 2\eta F/\alpha T_L^2} \quad (4)$$

where T_L is the lattice temperature. For high excitation fluences $T_e \gg T_L$ we then infer $\Delta T_e \propto F^{1/2}$. As it is illustrated in Fig. 3(a) our experimental data show a nonlinear dependence of the electron temperature on the excitation fluence that is scaling as $F^{1/2}$.

We now consider an intrinsic mechanism of cooling of the hot carriers in graphene. In graphene the strong electron–optical phonon coupling results in a very efficient channel that the hot carriers lose their energy by emission of optical phonons at the K and Γ points of the Brillouin zone with energies ~160 meV and 196 meV respectively, the so-called strong coupled optical phonons (SCOPs). The hot carriers with energy ≥160 meV can efficiently lose their energy through the electron–optical phonon interactions that results in a rapid decrease of their temperature T_e within few hundreds of femtoseconds. This produces a significant non equilibrium phonon population that subsequently decays towards lower energy acoustic phonon *via* anharmonic coupling.[39] In the case that the density of the emitted optical phonons is so high, then they cannot completely decay to low energy acoustic phonons, and a phonon bottleneck occurs. Part of their energy is reabsorbed by the electronic system that leads to an increase of the cooling time of graphene hot carriers. An important component in the intrinsic cooling process in graphene is the continuous rethermalization of the electronic gas. That means that the electrons with excess energy larger than the 0.16 eV above the Fermi energy have relaxed by coupling to SCOPs, the remaining electrons will thermalize through carrier–carrier scattering. That enables a continuous emission of optical phonons which operates as a continuous heat sink even at electron temperature of 300 K. The analytical model developed by Pogna *et. al.,*[56] captures the time evolution of this cooling channel. For carriers with excess energies <160 meV with respect the Fermi energy the hot carriers lose their energy by acoustic phonon emission with energy determined by $k_B T_{BG}$ per scattering event as it is determined by conservation of momentum. The T_{BG} is the Bloch–Gruneisen temperature[57] which is our case is calculated to be 98 K. Furthermore, Song *et al.,*[27] identified an unconventional, disorder-assisted electron-phonon mechanism that is highly efficient in cooling of carriers, and dominate in a wide range of temperatures. Since then, several groups have observed role of the supercollisions in the cooling process of the hot carriers in graphene.[41,42,44] The cooling times increases with decreasing the temperature from ~10 ps at 300 K to 200 ps below 50 K. In the high temperature limit $T_e \gg T_L$, that characterizes our experiment the time dependent electron temperature T_e is given by

$$T_e(t) = \frac{T_{e,0}}{1 + \frac{A}{\alpha}T_{e,0}t}, \quad T_e(t) \gg T_L \quad (5)$$

where $T_{e,0}$ is the initial electron temperature, $T_L = 295$ K is the lattice temperature, and the ratio $A/\alpha = 5.49 \times 10^7$ K^{-1} s^{-1} (the calculation of the ratio A/α is included in the ESI†).[27] Using the eqn (4) and (5) we calculated the time dependence of the electron temperature illustrated in Fig. 3(b). However, the dynamics of the photoinduced conductivity, shown in Fig. 2 and described by a single exponential form, is inconsistent with the temperature dynamics shown in Fig. 3(b). This leads us to the conclusion that the disorder assisted cooling is not the dominant cooling mechanism but can provide a parallel cooling channel of the carriers in time resolved THz spectroscopy experiments. Similarly, Mihnev *et. al.*,[25] also concluded that the disorder assisted cooling of carriers is not the primary cooling process for multilayer graphene. In Fig. 3(c) is depicted the cooling time as a function of the electron temperature. As the electron temperature increases, the cooling time increases as well. A similar trend of the decay time as a function of the excitation fluence has been also observed in chemical vapor deposition grown graphene.[21] A reasonable explanation is that the higher the temperature of the electrons, the longer it takes for them to cool down especially in the case that the Fermi energy is not near the charge neutrality point. The shift of the Fermi energy away from the charge neutrality point reflects large density of states that means higher electron heat capacity. Fig. 3(d) illustrates the maximum of the pump induced conductivity extracted from the data in Fig. 2(b). The increase of the conductivity maximum with the fluence is compatible with the corresponding increases of the electron temperatures as shown in Fig. 3(a). The relatively high pump fluence increases the Drude weight which is also expressed in terms of the density of the photogenerated carriers and gives rise to the conductivity. It is shown that the amplitude is ~ (fluence)$^{1/2}$ (solid yellow line) as it is expected. Furthermore, the lateral diffusion mechanism that also contribute to the relaxation process of the hot electron temperature is not relevant in the time scale of our measurements. The spot size of the excitation beam is ~2 mm so the lateral spreading of the excitation heat, despite the large in-plane diffusion rate occurs on a time scale much larger than the time scale we observed here. From the discussion above, we see that the dominant cooling process is the intrinsic cooling mechanism in which highly energetic hot carriers with energies >0.16 eV emit optical phonons.

In conclusion, we employed optical-pump THz-probe spectroscopy to investigate the cooling dynamics of hot carriers in quasi freestanding bilayer epitaxial grown graphene on SiC with H-intercalation. Considering negligible contribution of the substrate's optical phonons to the cooling process along with the inefficient cooling channel by supercollisions, we conclude that the cooling of carriers is primarily due to intrinsic mechanisms that involves the SCOPs and their subsequent relaxation by lower energy acoustic phonons. Interestingly, our results show a longer cooling time by more than twice the relaxation time observed in monolayer graphene in previous studies. This can be attributed to decoupling of the graphene layers form the SiC substrate due to the broken covalent bonds by the H intercalation. These results are important especially for opto-electronic devices based on quasi free-standing hydrogenated

epitaxial graphene as the hot carriers can retain their energy longer time before cooling down, which is pivotal for processes such as energy transfer, high-field electron transport, and thermoelectric effect.

Methods

Sample preparation

The growth of the bilayer graphene samples was conducted on a semi insulating 6H–SiC(0001), <0.2 deg off-axis substrate. Prior to growth, the sample was etched in H_2 during the ramp to growth temperature (1580 °C, 200 mbar) process to remove any polishing damage and prepare the surface for epitaxial graphene growth. Once the temperature was reached, epitaxial graphene was synthesized in 10 slm Ar at 100 mbar for 20 min. After growth, the sample was cooled to 1050 °C and H_2 replaced Ar to perform H intercalation using 80 slm H_2 at 950 mbar for 60 min. During the H intercalation process, the buffer layer which is present in epitaxial graphene converts to a second graphene layer, making a quasi-freestanding bilayer epitaxial graphene. A similar method used for the sample preparation in the work.[58] The Hall effect measurements of the graphene on semi-insulating SiC were performed on 8×8 mm^2 samples at room temperature in a van der Pauw configuration. Hall measurements are repeatable and known to be uniform ($\pm$10%) over samples synthesized on 100 mm substrates. These measurements are accepted by the graphene synthesis community.[58]

Author contributions

I. C. conceived and supervised the experiments, R. M. W. and D. K. G. synthesized the samples, and performed the hall measurements, I. C. and S. S. carried out the experiment, I. C. wrote the paper, and all authors contributed to improving the manuscript.

Conflicts of interest

There are no conflicts to declare.

Acknowledgements

Ioannis Chatzakis gratefully acknowledges the College of Art & Science, VPR office, and Provost office for their contribution to start-up funding and Rachael L. Myers-Word the financial support from the Office of Naval Research (ONR) for the research performed at the Naval Research Laboratory. We would also like to thank Paola Barbara at Georgetown University for her comments for improving this manuscript.

Notes and references

1 K. S. Novoselov, *et al.*, Two-dimensional gas of massless Dirac fermions in graphene, *Nature*, 2005, **438**, 197–200.
2 Y. Zhang, Y.-W. Tan, H. L. Stormer and P. Kim, Experimental observation of the quantum Hall effect and Berry's phase in graphene, *Nature*, 2005, **438**, 201–204.
3 K. I. Bolotin, *et al.*, Ultrahigh electron mobility in suspended graphene, *Solid State Commun.*, 2008, **146**, 351–355.
4 F. Bonaccorso, Z. Sun, T. Hasan and A. C. Ferrari, Graphene photonics and optoelectronics, *Nat. Photon*, 2010, **4**, 611–622.
5 P. Avouris, Graphene: Electronic and Photonic Properties and Devices, *Nano Lett.*, 2010, **10**, 4285–4294.
6 K. F. Mak, *et al.*, Measurement of the Optical Conductivity of Graphene, *Phys. Rev. Lett.*, 2008, **101**, 196405.
7 R. R. Nair, *et al.*, Fine Structure Constant Defines Visual Transparency of Graphene, *Science*, 2008, **320**, 1308.
8 J. M. Dawlaty, *et al.*, Measurement of the optical absorption spectra of epitaxial graphene from terahertz to visible, *Appl. Phys. Lett.*, 2008, **93**, 131905.
9 H. Yan, *et al.*, Infrared Spectroscopy of Wafer-Scale Graphene, *ACS Nano*, 2011, **5**, 9854–9860.
10 M. C. Lemme, T. J. Echtermeyer, M. Baus and H. Kurz, A Graphene Field-Effect Device, *IEEE Electron Device Lett.*, 2007, **28**, 282–284.
11 M. Jablan, H. Buljan and M. Soljačić, Plasmonics in graphene at infrared frequencies, *Phys. Rev. B: Condens. Matter Mater. Phys.*, 2009, **80**, 245435.
12 Y.-M. Lin, *et al.*, 100-GHz Transistors from Wafer-Scale Epitaxial Graphene, *Science*, 2010, **327**, 662.
13 L. Ju, *et al.*, Graphene plasmonics for tunable terahertz metamaterials, *Nat. Nanotechnol.*, 2011, **6**, 630–634.
14 L. Liao, *et al.*, High-speed graphene transistors with a self-aligned nanowire gate, *Nature*, 2010, **467**, 305–308.
15 Q. Bao and K. P. Loh, Graphene Photonics, Plasmonics, and Broadband Optoelectronic Devices, *ACS Nano*, 2012, **6**, 3677–3694.
16 S.-F. Shi, *et al.*, Controlling Graphene Ultrafast Hot Carrier Response from Metal-like to Semiconductor-like by Electrostatic Gating, *Nano Lett.*, 2014, **14**, 1578–1582.
17 A. Tomadin, *et al.*, The ultrafast dynamics and conductivity of photoexcited graphene at different Fermi energies, *Sci. Adv.*, 2018, **4**, eaar5313.
18 G. Jnawali, Y. Rao, H. Yan and T. F. Heinz, Observation of a Transient Decrease in Terahertz Conductivity of Single-Layer Graphene Induced by Ultrafast Optical Excitation, *Nano Lett.*, 2013, **13**, 524–530.
19 P. A. George, *et al.*, Ultrafast Optical-Pump Terahertz-Probe Spectroscopy of the Carrier Relaxation and Recombination Dynamics in Epitaxial Graphene, *Nano Lett.*, 2008, **8**, 4248–4251.
20 S. Kar, D. R. Mohapatra, E. Freysz and A. K. Sood, Tuning photoinduced terahertz conductivity in monolayer graphene: Optical-pump terahertz-probe spectroscopy, *Phys. Rev. B: Condens. Matter Mater. Phys.*, 2014, **90**, 165420.
21 T. Jia, *et al.*, Role of the Optical–Acoustic Phonon Interaction in the Ultrafast Cooling Process of CVD Graphene, *J. Phys. Chem. C*, 2021, **125**, 27283–27289.
22 S. Kar, S. Jayanthi, E. Freysz and A. K. Sood, Time resolved terahertz spectroscopy of low frequency electronic

resonances and optical pump-induced terahertz photoconductivity in reduced graphene oxide membrane, *Carbon*, 2014, **80**, 762–770.

23 L. Luo, I. Chatzakis, A. Patz and J. Wang, Ultrafast Terahertz Probes of Interacting Dark Excitons in Chirality-Specific Semiconducting Single-Walled Carbon Nanotubes, *Phys. Rev. Lett.*, 2015, **114**, 107402.

24 T. Kampfrath, L. Perfetti, F. Schapper, C. Frischkorn and M. Wolf, Strongly Coupled Optical Phonons in the Ultrafast Dynamics of the Electronic Energy and Current Relaxation in Graphite, *Phys. Rev. Lett.*, 2005, **95**, 187403.

25 M. T. Mihnev, *et al.*, Electronic cooling *via* interlayer Coulomb coupling in multilayer epitaxial graphene, *Nat. Commun.*, 2015, **6**, 8105.

26 R. Bistritzer and A. H. MacDonald, Electronic Cooling in Graphene, *Phys. Rev. Lett.*, 2009, **102**, 206410.

27 J. C. W. Song, M. Y. Reizer and L. S. Levitov, Disorder-Assisted Electron-Phonon Scattering and Cooling Pathways in Graphene, *Phys. Rev. Lett.*, 2012, **109**, 106602.

28 J. C. Johannsen, *et al.*, Direct View of Hot Carrier Dynamics in Graphene, *Phys. Rev. Lett.*, 2013, **111**, 027403.

29 T. Low, V. Perebeinos, R. Kim, M. Freitag and P. Avouris, Cooling of photoexcited carriers in graphene by internal and substrate phonons, *Phys. Rev. B: Condens. Matter Mater. Phys.*, 2012, **86**, 045413.

30 S. Winnerl, *et al.*, Carrier Relaxation in Epitaxial Graphene Photoexcited Near the Dirac Point, *Phys. Rev. Lett.*, 2011, **107**, 237401.

31 J. N. Heyman, *et al.*, Carrier heating and negative photoconductivity in graphene, *J. Appl. Phys.*, 2015, **117**, 015101.

32 D. Sun, *et al.*, Spectroscopic Measurement of Interlayer Screening in Multilayer Epitaxial Graphene, *Phys. Rev. Lett.*, 2010, **104**, 136802.

33 I. Gierz, *et al.*, Snapshots of non-equilibrium Dirac carrier distributions in graphene, *Nat. Mater.*, 2013, **12**, 1119–1124.

34 J. M. Dawlaty, S. Shivaraman, M. Chandrashekhar, F. Rana and M. G. Spencer, Measurement of ultrafast carrier dynamics in epitaxial graphene, *Appl. Phys. Lett.*, 2008, **3**, 042116.

35 M. R. Amer, A. Bushmaker and S. B. Cronin, The Influence of Substrate in Determining the Band Gap of Metallic Carbon Nanotubes, *Nano Lett.*, 2012, **12**, 4843–4847.

36 M. Massicotte, G. Soavi, A. Principi and K.-J. Tielrooij, Hot carriers in graphene – fundamentals and applications, *Nanoscale*, 2021, **13**, 8376–8411.

37 T. Li, *et al.*, Femtosecond Population Inversion and Stimulated Emission of Dense Dirac Fermions in Graphene, *Phys. Rev. Lett.*, 2012, **108**, 167401.

38 J. H. Strait, *et al.*, Very Slow Cooling Dynamics of Photoexcited Carriers in Graphene Observed by Optical-Pump Terahertz-Probe Spectroscopy, *Nano Lett.*, 2011, **11**, 4902–4906.

39 I. Chatzakis, H. Yan, D. Song, S. Berciaud and T. F. Heinz, Temperature dependence of the anharmonic decay of optical phonons in carbon nanotubes and graphite, *Phys. Rev. B: Condens. Matter Mater. Phys.*, 2011, **83**, 205411.

40 A. C. Betz, *et al.*, Hot Electron Cooling by Acoustic Phonons in Graphene, *Phys. Rev. Lett.*, 2012, **109**, 056805.

41 A. C. Betz, *et al.*, Supercollision cooling in undoped graphene, *Nat. Phys.*, 2013, **9**, 109–112.

42 M. W. Graham, S.-F. Shi, D. C. Ralph, J. Park and P. L. McEuen, Photocurrent measurements of supercollision cooling in graphene, *Nat. Phys.*, 2013, **9**, 103–108.

43 T. V. Alencar, M. G. Silva, L. M. Malard and A. M. de Paula, Defect-Induced Supercollision Cooling of Photoexcited Carriers in Graphene, *Nano Lett.*, 2014, **14**, 5621–5624.

44 A. El Fatimy, *et al.*, Effect of defect-induced cooling on graphene hot-electron bolometers, *Carbon*, 2019, **154**, 497–502.

45 V. Perebeinos and P. Avouris, Inelastic scattering and current saturation in graphene, *Phys. Rev. B: Condens. Matter Mater. Phys.*, 2010, **81**, 195442.

46 K. J. Tielrooij, *et al.*, Photoexcitation cascade and multiple hot-carrier generation in graphene, *Nat. Phys.*, 2013, **9**, 248–252.

47 S. Winnerl, *et al.*, Time-resolved spectroscopy on epitaxial graphene in the infrared spectral range: relaxation dynamics and saturation behavior, *J. Phys.: Condens. Matter*, 2013, **25**, 054202.

48 J. D. Emery, *et al.*, Structural consequences of hydrogen intercalation of epitaxial graphene on SiC(0001), *Appl. Phys. Lett.*, 2014, **105**, 161602.

49 S. Forti and U. Starke, Epitaxial graphene on SiC: from carrier density engineering to quasi-free standing graphene by atomic intercalation, *J. Phys. D: Appl. Phys.*, 2014, **47**, 094013.

50 C. Riedl, C. Coletti, T. Iwasaki, A. A. Zakharov and U. Starke, Quasi-Free-Standing Epitaxial Graphene on SiC Obtained by Hydrogen Intercalation, *Phys. Rev. Lett.*, 2009, **103**, 246804.

51 S. Forti, *et al.*, Large-area homogeneous quasifree standing epitaxial graphene on SiC(0001): Electronic and structural characterization, *Phys. Rev. B: Condens. Matter Mater. Phys.*, 2011, **84**, 125449.

52 J. Hass, *et al.*, Why Multilayer Graphene on 4 H − SiC (0001) Behaves Like a Single Sheet of Graphene, *Phys. Rev. Lett.*, 2008, **100**, 125504.

53 J. Ristein, S. Mammadov and Th. Seyller, Origin of Doping in Quasi-Free-Standing Graphene on Silicon Carbide, *Phys. Rev. Lett.*, 2012, **108**, 246104.

54 J. L. Tedesco, *et al.*, Hall effect mobility of epitaxial graphene grown on silicon carbide, *Appl. Phys. Lett.*, 2009, **95**, 122102.

55 F. Speck, *et al.*, The quasi-free-standing nature of graphene on H-saturated SiC(0001), *Appl. Phys. Lett.*, 2011, **99**, 122106.

56 E. A. A. Pogna, *et al.*, Hot-Carrier Cooling in High-Quality Graphene Is Intrinsically Limited by Optical Phonons, *ACS Nano*, 2021, **15**, 11285–11295.

57 J. K. Viljas and T. T. Heikkilä, Electron-phonon heat transfer in monolayer and bilayer graphene, *Phys. Rev. B: Condens. Matter Mater. Phys.*, 2010, **81**, 245404.

58 K. M. Daniels, *et al.*, Narrow plasmon resonances enabled by quasi-freestanding bilayer epitaxial graphene, *2D Mater.*, 2017, **4**, 025034.